IOPscience iopscience.iop.org

Home Search Collections Journals About Contact us My IOPscience

A FIB induced boiling mechanism for rapid nanopore formation

This content has been downloaded from IOPscience. Please scroll down to see the full text.

2014 Nanotechnology 25 035303

(http://iopscience.iop.org/0957-4484/25/3/035303)

View the table of contents for this issue, or go to the journal homepage for more

Download details:

IP Address: 130.126.32.13
This content was downloaded on 21/12/2013 at 04:42

Please note that terms and conditions apply.

IOP Publishing Nanotechnology

Nanotechnology **25** (2014) 035303 (5pp) doi:10.1088/0957-4484/25/3/035303

A FIB induced boiling mechanism for rapid nanopore formation

K Das[1], J B Freund[1,2] and H T Johnson[1]

[1] Department of Mechanical Science and Engineering, University of Illinois at Urbana-Champaign, 1206 West Green Street, MC-244, Urbana, IL 61801, USA
[2] Department of Aerospace Engineering, University of Illinois at Urbana-Champaign, 306 Talbot Laboratory, MC-236, 104 South Wright Street Urbana, IL 61801, USA

E-mail: das7@illinois.edu, jbfreund@illinois.edu and htj@illinois.edu

Received 18 October 2013, revised 25 November 2013
Accepted for publication 28 November 2013
Published 20 December 2013

Abstract

Focused ion beam (FIB) technology is widely used to fabricate nanopores in solid-state membranes. These nanopores have desirable thermomechanical properties for applications such as high-throughput DNA sequencing. Using large scale molecular dynamics simulations of the FIB nanopore formation process, we show that there is a threshold ion delivery rate above which the mechanism underlying nanopore formation changes. At low rates nanopore formation is slow, with the rate proportional to the ion flux and therefore limited by the sputter rate of the target material. However, at higher fluxes nanopores form via a thermally dominated process, consistent with an explosive boiling mechanism. In this case, mass is rapidly rearranged via bubble growth and coalescence, much more quickly than would occur during sputtering. This mechanism has the potential to greatly speed up nanopore formation.

Keywords: atomistic simulations, focused ion beam simulation, nanopore fabrication, explosive boiling

(Some figures may appear in colour only in the online journal)

1. Introduction

Nanopores in thin solid-state membranes have extraordinary potential applications in biosensing and DNA sequencing [1–3], offering better mechanical properties and higher thermal robustness than nanopores in biological membranes. They also have better chemical stability, superior dimensional control, and may be easily integrated into devices [4]. Molecular receptors can be added around the sides of a nanopore to provide biochemical selectivity, thus enabling label-free analysis of proteins [5]. Recently, focused ion beam (FIB) processing has shown promise in the formation of solid-state nanopores [6, 7] with diameters less than 5 nm [8], though the hole 'drilling' mechanisms are not yet well understood.

The standard view of FIB machining is that it is predominantly a sputter erosion process [9]. Energetic ions are understood to impact the target surface and impart kinetic energy to the nearby target atoms. When the atoms near the surface obtain sufficient kinetic energy, they are sputtered. For typical operating conditions, each ion sputters approximately 2–3 target atoms depending on the ion beam energy and incidence angle [10]. Thus, successive ion impacts from a focused ion beam on a thin membrane target will eventually create a nanopore. In this view, the process is mostly mechanical, with ions knocking atoms off a surface without significant heating.

While formation of solid-state nanopores using FIB provides better control of pore diameter than chemical etching methods commonly used as alternatives to FIB (e.g. feedback chemical etching [11], ion track etching [12, 13]), under typical conditions (beam current $I = 30$ pA [14]) FIB is inherently slow, and it may require several seconds to fabricate a single nanopore [7, 8, 15] through a 100 nm thick membrane. However, here we show for the first time that under slightly higher ion fluxes, which exceed a critical value (flux $f \geq 1.8 \times 10^{24}$ cm^{-2} s^{-1}), nanopore formation changes over to a thermally dominated process,

 © 2014 IOP Publishing Ltd Printed in the UK

in which explosive boiling of the target material controls nanopore formation mechanics through material removal and rearrangement. According to prior estimates [14], these fluxes would correspond to beam currents of 225 pA and higher, which are approximately a factor of 10 higher than typical experimental conditions. We note that a precise conversion from ion beam flux to current is difficult due to uncertainty in the extent of charge neutralization in such beams [16–18]. Without accounting for charge neutralization, one would typically find a three order of magnitude difference between flux and inferred current [19–21], (and thus the assertion that with charge neutralization 1.8×10^{24} cm^{-2} s^{-1} is equivalent to approximately 225 pA) but we refer to flux in the present work because it is neutralization independent and can thus be precisely calculated. In the high flux regime, nanopore formation is orders of magnitude faster, occurring within tens of picoseconds, and it becomes independent of ion beam flux. The deposited energy flux far exceeds the thermal energy conduction into the target material, and temperature increases to a point at which nanopore formation is achieved by a phase change mechanism.

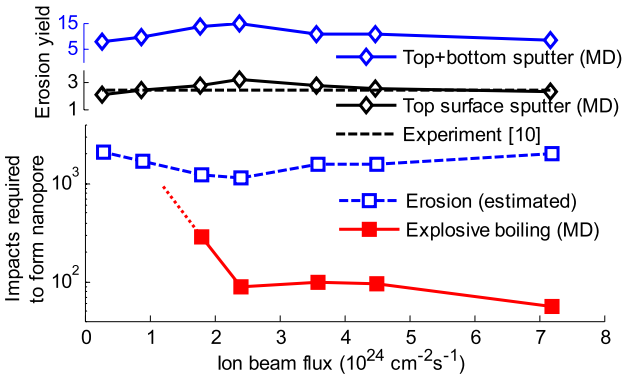

Figure 1. A critical ion beam flux for rapid nanopore formation via explosive boiling. The number of ion impacts required for nanopore formation via sputter erosion (top frame) is insensitive to the ion beam flux (open symbols). However, nanopore formation, as computed directly via MD, is nearly two orders of magnitude faster when beam flux is greater than about 1.8×10^{24} cm^{-2} s^{-1} (closed symbols).

2. Methods

To demonstrate this we model high flux, 50 keV, 3.5 nm FWHM (full width at half maximum) Ga FIB using molecular dynamics (MD) simulation, with the goal of simulating nanopore formation. A custom MD code [22] is used for these simulations. This code has successfully predicted experimental sputter yield and ripple formation in ion bombarded silicon [23, 24]. The incoming ion flux is varied by changing the time interval between impacts, ranging from 0.5 to 12 ps (7.2×10^{24} cm^{-2} s^{-1} $> f >$ 3.0×10^{23} cm^{-2} s^{-1}). An 11 nm thick free-standing silicon membrane is modeled using the Stillinger–Weber [25] potential for Si–Si interactions and a Molière [26] potential for Ga–Ga and Ga–Si interactions. A free-standing film of 27×27 nm^2 lateral extent, with fixed and thermostatically cooled lateral sides, is modeled. Results are independent of this lateral dimension.

3. Results and discussion

According to the conventional view, sputtering drives nanopore formation. We use sputter erosion theory to estimate the number of ion impacts required to form a typical nanopore and compare the estimate to the results of our high flux MD simulations. Using a measured sputter yield value of 2.5 atoms/ions [10], which matches closely our MD calculated sputter yield, (figure 1, top), we find that the number of impacts to nanopore formation is 6×10^3 (requiring a time of 3×10^3 ps) for the highest flux case ($f = 7.2\times10^{24}$ cm^{-2} s^{-1}) considered here. We note that there is a small variation in the MD calculated sputter yield relative to the experimental sputter yield due to inhomogeneity in the surface as erosion occurs. On the other hand, the full molecular dynamics calculation shows that a nanopore forms much faster than the sputter erosion theory predicts (after only 55 impacts or 27.5 ps, also shown in figure 1). We note that sputter yields are only weakly dependent on flux, so this does not explain the remarkable accelerated nanopore formation. Also, accounting for atoms sputtered from both the top and bottom surfaces of the film makes no significant change in the sputter erosion prediction, reducing it to 1×10^3 ps, which is still nearly two orders of magnitude higher than observed in the high flux MD simulations. Thus, a sputter erosion mechanism fails to explain the accelerated nanopore formation under modestly higher FIB fluxes.

In high flux FIB there is insufficient time for absorbed thermal energy to dissipate into the bulk target material which leads to a runaway thermal nanopore formation process. This mechanism shares features with explosive boiling [27], the violent phase change that can occur in rapidly heated liquid. Our results show that this phenomenon becomes the dominant mechanism for nanopore formation in high flux FIB. Next, we focus on the temperature of the target center and present evidence of explosive boiling as a material removal/rearrangement mechanism.

The flux dependence of the target temperature and relative RMS density ($\rho_{\mathrm{rms}}/\rho_{\mathrm{relative}}$), shown in figure 2, is consistent with an explosive boiling mechanism. Temperature is averaged over a 2 nm radius cylinder beneath the 3.5 nm FWHM ion beam between the 200th and 400th ion impacts, thus starting once the radial temperature distribution is statistically stable for all cases. During this interval, energy deposited in the target is conducted to the lateral sides and removed by the MD thermostats, modeling conduction into a larger film. In the high flux cases ($f \geq 1.8 \times 10^{24}$ cm^{-2} s^{-1}), the center of the target reaches temperatures much higher than the boiling point of silicon, and approaching the critical temperature (estimated to be over 6000 K for Stillinger–Weber silicon [28]).

When the heat flux is high, there is insufficient time for the system to follow the equilibrium 'liquid–vapor' (binodal) line, as dictated by the Clausius–Clapeyron relation, for which the relaxation time is on the order of nanoseconds [29]. For

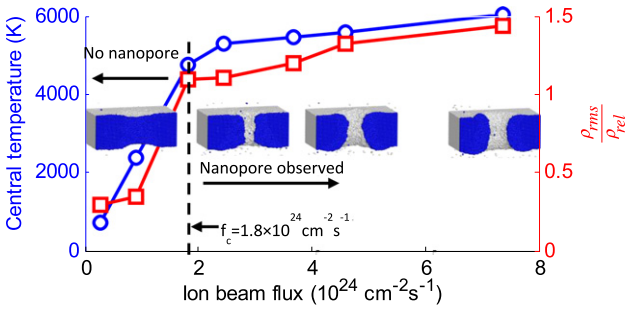

Figure 2. Temperature and relative RMS density near the center of the target, as a function of beam flux. Results are averaged between the 200th and 400th impact, when the system reaches steady state in all cases. With increasing ion flux, the temperature in the target increases, approaching the critical temperature of silicon. Large fluctuations in relative density are seen above the same threshold in ion flux. Together, these observations suggest a switchover to an explosive boiling mechanism.

the highest flux case, ions arrive every 0.5 ps while the relevant relaxation time for the temperature of a local spot (2 nm) to fall below melting point is approximately 2 ps as dictated by the thermal spike model [30]. As a result, the temperature of the system rapidly approaches the critical temperature [27, 31, 32]. The system becomes a superheated liquid, approaching the spinodal boundary associated with instability to phase decomposition, and large fluctuations in density, specific heat, entropy, and pressure become possible. Indeed, large density fluctuations are observed in the relative RMS density, shown in figure 2; these fluctuations exceed unity for the high flux cases. Spontaneous nucleation of bubble-like vapor-filled regions occurs, converting thermal energy to surface energy and preventing the system from reaching the spinodal boundary. As shown in figure 3, these bubbles grow and merge, resulting in a nanopore. This explosive boiling process is only observed in the high flux cases. Low flux cases show only slow erosion, which cannot be simulated long enough via MD to observe the complete nanopore formation process.

Two alternative pathways are therefore possible for nanopore formation: sputter erosion at low flux, and explosive boiling at high flux. Figure 3 (top) shows the sputter erosion mechanism, whereby atoms are displaced from the top and bottom surfaces by the incident ions during low flux FIB machining. In the low flux regime, the rate of nanopore formation is proportional to the flux. Figure 3 also shows the explosive boiling mechanism (bottom) that occurs in high flux FIB machining, with images taken from the molecular dynamics simulations. The absorbed thermal energy is rapidly converted to new surface area in the form of bubbles, which coalesce and rupture, quickly creating a through-thickness nanopore in tens of picoseconds. Explosive boiling thus facilitates rapid nanopore formation during high flux FIB processing. The two pathways can be viewed as alternative pathways for overcoming an energy barrier associated with nanopore formation.

During sputter erosion, incoming ions slowly erode the top and bottom surfaces, converting the kinetic energy of the incident ions into new surface energy in the system. During this process, the surface energy increases continuously until it reaches a peak value just prior to formation of the nanopore; after the nanopore opens, the surface relaxes, reducing the surface energy of the system. An equivalent energy barrier can be overcome much faster, instead, via the explosive boiling mechanism. The addition of energy to the system in high flux FIB rapidly raises the temperature of the system. The energy is then converted to surface energy in the form of bubbles; the system energy reaches a maximum before the nanopore forms, and the system then relaxes to the same final nanopore configuration as would be achieved via sputter erosion.

We can calculate the surface energy history for both pathways. For the slow sputtering process, we assume a parameterized geometry corresponding to the dashed lines in figure 3 (top). The energy history associated with this

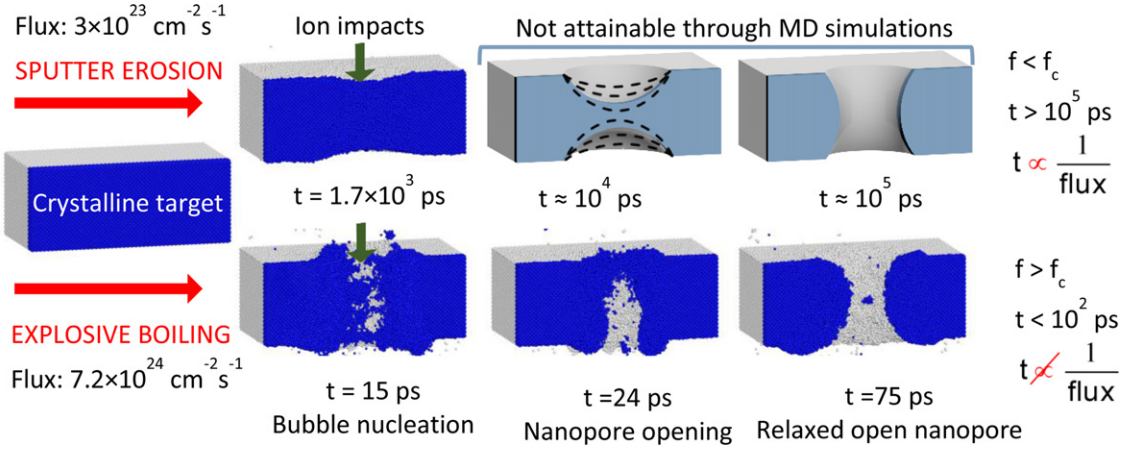

Figure 3. Two alternative pathways for nanopore formation. Top: following conventional sputter erosion theory, the time required for nanopore formation is proportional to the ion flux, and the process is much too slow to compute directly via MD. Bottom: following the explosive boiling mechanism, the time required for formation is insensitive to ion flux and is typically over 100 times faster than in the sputter erosion case.

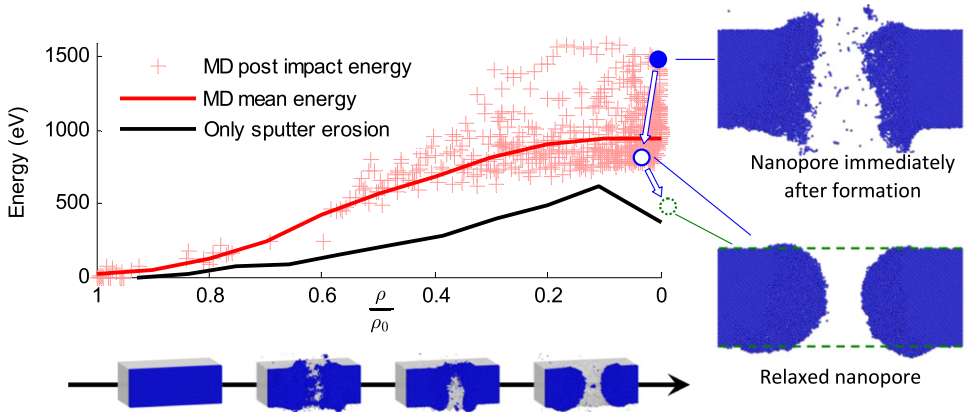

Figure 4. Energy of the target at various times, as a function of the relative density in the center of the target. The time sequence moves approximately from left to right as the nanopore forms. Shortly after a nanopore opens, the nanopore morphology relaxes to a smoother, lower energy configuration (filled circle to open circle). If the rim surrounding the nanopore were not considered, the MD-based energy (red curve) would better match the final point in the sputter erosion history (black curve).

evolving geometry, features a maximum prior to nanopore formation, as shown in figure 4. For high flux cases, also shown in figure 4, the energy of the system is monitored directly in the MD simulation by measuring the surface area of the interfaces of atoms and low-density vapor, considering all free surfaces including the bubbles that nucleate in the membrane. Relative density, which tracks the formation of the nanopore, is computed by considering a 2 nm radius cylinder at the center of the membrane. The time history proceeds approximately from left (high density, or absence of nanopore) to right (low density, or presence of nanopore).

From sputter erosion theory, a stable nanopore of the size considered here has surface energy of approximately 450 eV in excess of that of the target crystalline film. The black curve in figure 4 shows the evolving surface energy during sputter erosion. The approximate geometric analysis shows that during sputter erosion, the excess surface energy of the system slowly increases to 600 eV, after which the nanopore opens and the excess surface energy relaxes to 450 eV. Results show that during the high flux MD simulation, the excess surface energy of the membrane with bubbles inside reaches as high as 1500 eV very rapidly, far exceeding the slow-process energy barrier. Two representative atomistic configurations observed during high flux FIB are also shown in figure 4. The first configuration represents a highly energetic state immediately after formation of the nanopore. After a few more ion impact times (about 20 ps for this case), the configuration relaxes as expected to a correspondingly lower surface energy as shown (moving from the filled circle to open circle in figure 4).

We observe significant material rearrangement just after a nanopore opens. The explosive boiling process forces atoms near the center to move radially outward and toward the free surfaces at the top and bottom of the film. Mass rearrangement occurs around the top and bottom surfaces of the film, and results in the formation of raised rims. During this short time, far more material is rearranged than sputtered. At typical sputter yields, less than 5% of the nearly 16 000 atoms making up the volume of the nanopore could have been removed by sputtering. We note that since some mass is rearranged to form the raised rims of the nanopore, the actual nanopore structure will have higher energy than a nanopore formed by thinning due to sputter erosion alone. Excluding the rim volume from the calculation of MD surface energy brings the excess surface energy down to less than 500 eV, as shown by the dotted circle in figure 4.

4. Conclusions

In summary, we show that very rapid nanopore formation is possible, with a modest increase in flux above the typical experimental levels, via a FIB induced boiling mechanism. During high flux FIB, sputter erosion rates do not limit nanopore formation speed, and the formation rate of the nanopore is no longer proportional to ion flux as it is during low flux FIB. A thermal effect, observed to be consistent with explosive boiling, is found to be the dominant mechanism at high fluxes. An energy barrier is required to achieve nanopore formation; in the high flux case the barrier is overcome through the increase in surface energy associated with the formation, coalescence, and rupture of bubbles in the target material. A raised rim around the nanopore is evidence of significant mass rearrangement that occurs during nanopore formation, which is again consistent with the observed explosive boiling mechanism. Operating at fluxes near the threshold of explosive boiling may affect process control for some FIB applications.

Acknowledgment

The authors gratefully acknowledge the support of NSF grant no. CMMI-0825173.

References

[1] Xie P, Xiong Q, Fang Y, Qing Q and Lieber C M 2011 Local electrical potential detection of DNA by nanowire–nanopore sensors *Nature Nanotechnol.* **7** 119–25

[2] Martin C R and Siwy Z S 2007 Learning nature's way: biosensing with synthetic nanopores *Science* **317** 331–2
[3] Mussi V, Fanzio P, Repetto L, Firpo G, Scaruffi P, Stigliani S and Valbusa U 2010 DNA-functionalized solid state nanopore for biosensing *Nanotechnology* **21** 145102
[4] Dekker C 2007 Solid-state nanopores *Nature Nanotechnol.* **2** 209–15
[5] Wei R, Gatterdam V, Wieneke R, Tampé R and Rant U 2012 Stochastic sensing of proteins with receptor-modified solid-state nanopores *Nature Nanotechnol.* **7** 257–63
[6] Li J, Stein D, McMullan C, Branton D, Aziz M J and Golovchenko J A 2001 Ion-beam sculpting at nanometre length scales *Nature* **412** 166–9
[7] Lanyon Y H, De Marzi G, Watson Y E, Quinn A J, Gleeson J P, Redmond G and Arrigan D W 2007 Fabrication of nanopore array electrodes by focused ion beam milling *Anal. Chem.* **79** 3048–55
[8] Lo C J, Aref T and Bezryadin A 2006 Fabrication of symmetric sub-5 nm nanopores using focused ion and electron beams *Nanotechnology* **17** 3264
[9] Giannuzzi L A and Stevie F A 1999 A review of focused ion beam milling techniques for TEM specimen preparation *Micron* **30** 197–204
[10] Lugstein A, Basnar B, Smoliner J and Bertagnolli E 2003 FIB processing of silicon in the nanoscale regime *Appl. Phys.* A **76** 545–8
[11] Park S R, Peng H and Ling X S 2007 Fabrication of nanopores in silicon chips using feedback chemical etching *Small* **3** 116–9
[12] Siwy Z, Dobrev D, Neumann R, Trautmann C and Voss K 2003 Electro-responsive asymmetric nanopores in polyimide with stable ion-current signal *Appl. Phys.* A **76** 781–5
[13] Apel P Y, Korchev Y E, Siwy Z, Spohr R and Yoshida M 2001 Diode-like single-ion track membrane prepared by electro-stopping *Nucl. Instrum. Methods Phys. Res.* B **184** 337–46
[14] MoberlyChan W J 2009 Dual-beam focused ion beam/electron microscopy processing and metrology of redeposition during ion–surface 3D interactions, from micromachining to self-organized picostructures *J. Phys.: Condens. Matter* **21** 224013
[15] Patterson N, Adams D P, Hodges V C, Vasile M J, Michael J R and Kotula P G 2008 Controlled fabrication of nanopores using a direct focused ion beam approach with back face particle detection *Nanotechnology* **19** 235304
[16] Goncharov A 2013 Invited review article: the electrostatic plasma lens *Rev. Sci. Instrum.* **84** 021101
[17] Stevie F A, Giannuzzi L A and Prenitzer B I 2005 *Introduction to Focused Ion Beams: Instrumentation, Theory, Techniques and Practice* (New York: Springer)
[18] Volkert C A and Minor A M 2007 Focused ion beam microscopy and micromachining *MRS Bull.* **32** 389–95
[19] Matovic J, Kettle J, Brousseau E and Adamovic N 2008 Patterning of nanomembranes with a focused-ion-beam *Microelectronics MIEL 26th Int. Conf.* pp 103–6
[20] Kolíbal M, Matlocha T, Vystavěl T and Šikola T 2011 Low energy focused ion beam milling of silicon and germanium nanostructures *Nanotechnology* **22** 105304
[21] Liu Y, Longo D M and Hull R 2003 Ultrarapid nanostructuring of poly (methylmethacrylate) films using Ga^{+} focused ion beams *Appl. Phys. Lett.* **82** 346–8
[22] Hossain M Z, Das K, Freund J B and Johnson H T 2011 Ion impact crater asymmetry determines surface ripple orientation *Appl. Phys. Lett.* **99** 151913
[23] Moore M C, Kalyanasundaram N, Freund J B and Johnson H T 2004 Structural and sputtering effects of medium energy ion bombardment of silicon *Nucl. Instrum. Methods Phys. Res.* B **225** 241–55
[24] Kalyanasundaram N, Freund J B and Johnson H T 2009 A multiscale crater function model for ion-induced pattern formation in silicon *J. Phys.: Condens Matter* **21** 224018
[25] Stillinger F H and Weber T A 1985 Computer simulation of local order in condensed phases of silicon *Phys. Rev.* B **31** 5262
[26] Moliere G 1947 Theory of scattering of fast charged particles. I, single scattering in a screened Coulomb field *Z. Naturf.* a **2** 133
[27] Martynyuk M M 1977 Phase explosion of a metastable fluid *Combust., Explosion Shock Waves* **13** 178–91
[28] Honda N and Nagasaka Y 1999 Vapor–liquid equilibria of silicon by the Gibbs ensemble simulation *Int. J. Thermophys.* **20** 837–46
[29] Skripov V P 1974 *Metastable Liquids* (New York: Wiley)
[30] de la Rubia D, Averback R S, Hsieh H and Benedek R 1989 Molecular dynamics simulation of displacement cascades in Cu and Ni: thermal spike behavior *J. Mater. Res.* **4** 579–86
[31] Yoo J H, Jeong S H, Mao X L, Greif R and Russo R E 2000 Evidence for phase-explosion and generation of large particles during high power nanosecond laser ablation of silicon *Appl. Phys. Lett.* **76** 783–5
[32] Miotello A and Kelly R 1995 Critical assessment of thermal models for laser sputtering at high fluences *Appl. Phys. Lett.* **67** 3535–7